Chemical Engineering Journal 480 (2024) 147968

Contents lists available at ScienceDirect

Chemical Engineering Journal

journal homepage: www.elsevier.com/locate/cej

Experimental study and comprehensive kinetic modeling of the direct dimethyl ether synthesis on Cu/ZnO/ZrO_2 and H-FER-20

Gabriela Rodrigues Niquini, Bruno Lacerda de Oliveira Campos, Karla Herrera Delgado *, Stephan Pitter, Jörg Sauer

Institute of Catalysis Research and Technology (IKFT), Karlsruhe Institute of Technology (KIT), Hermann-von Helmholtz-Platz 1, D-76344 Eggenstein-Leopoldshafen, Germany

ARTICLE INFO

Keywords:
Reaction kinetics
Direct dimethyl ether synthesis
Dual catalyst system
Syngas

ABSTRACT

In the direct dimethyl ether (DME) synthesis, the combination of Cu/ZnO/ZrO_2 (CZZ) and H-FER-20 (FER) has shown high selectivity and productivity for a broad range of CO_2/CO_X ratio. Aiming to understand the behavior of the studied catalyst system under distinct operating conditions, we developed a new 9-parameter kinetic model. The parameters were estimated based on 815 steady-state experiments carried out at several values of pressure (30–54 bar), temperature (190–250 °C), space-velocity (0.79–4.34 s^{-1}) and inlet gas composition. This broad database was used in the development and validation of a new 9-parameter kinetic model for the direct DME synthesis. The model adequately simulates experiments in several process conditions, with 95% of the simulated points presenting a deviation lower than 20% with respect to the experimental results for outlet DME molar percentage. In addition, it correctly predicts the trends with respect to variations in H_2 inlet fraction, which is of high relevance for processes using fluctuating renewable power sources for H_2 production. In comparison to state-of-the-art models with more parameters, the new model is significantly more accurate. It benefits from the broad range of validity and elevated number of experimental points, which makes it a reliable model that can be applied for process optimization and scale-up.

1. Introduction

The production and utilization of green hydrogen, generated from electrolysis operated with solar or wind power, is one of the keys for our future energy system and for enabling sustainable production processes [1]. However, the low volumetric energy content of H_2 limits its application in the transportation section to large vehicles and makes its storage more expensive than other fuels [2]. Besides, for the implementation of a so-called hydrogen economy, the infrastructure to transport and store H_2 is yet to be constructed [3]. To overcome these difficulties, hydrogen can be chemically stored by conversion with CO and CO_2 in so-called Power-to-X (PtX) routes. This approach yields liquid organic compounds of higher energy density, suitable to be transported and stored in the existing infrastructure for carbon-containing fossil fuels [4,5].

Among PtX products, dimethyl ether (DME) is promising for use in the chemical industry and transportation sector [6]. It is a feedstock to produce light olefins, oxymethylene ethers and gasoline, among other synthetic hydrocarbons. It is also an alternative fuel, due to its high cetane number and cleaner combustion product, with low soot emission and reduced CO, hydrocarbons and NO_x emissions comparing to diesel [7,8].

Commercially, DME is produced from syngas in two stages, under the presence of a functional catalyst in each step. In the first stage, CO and CO_2 react with hydrogen to form methanol (Reactions (1) and (2)), in parallel with the reverse water–gas shift (rWGSR, Reaction (3)) as side reaction. In the second stage, methanol undergoes dehydration to form DME (Reaction (4)).

$$CO + 2H_2 \rightleftharpoons CH_3OH \quad \Delta H^0_{25^\circ C} = -90.4 kJ \cdot mol^{-1} \tag{1}$$

$$CO_2 + 3H_2 \rightleftharpoons CH_3OH + H_2O \quad \Delta H^0_{25^\circ C} = -49.4 kJ \cdot mol^{-1} \tag{2}$$

$$CO_2 + H_2 \rightleftharpoons CO + H_2O \quad \Delta H^0_{25^\circ C} = +41.0 kJ \cdot mol^{-1} \tag{3}$$

$$2\,CH_3OH \rightleftharpoons CH_3OCH_3 + H_2O \quad \Delta H^0_{25^\circ C} = -23.5\,kJ \cdot mol^{-1} \tag{4}$$

* Corresponding author.
E-mail address: karla.herrera@kit.edu (K. Herrera Delgado).

https://doi.org/10.1016/j.cej.2023.147968
Received 12 September 2023; Received in revised form 17 November 2023; Accepted 6 December 2023
Available online 13 December 2023

The synthesis of DME in one reactor over a dual catalyst system allows to overcome the thermodynamic limitations of methanol synthesis (Reactions (1) and (2)), since methanol is consumed *in situ* via Reaction (4), lowering its concentration and driving the reaction towards the generation of products. Additionally, the installation of a single reactor might lead to lower investment costs [5,9]. Due to these advantages, DME direct synthesis is in focus and already being investigated in pilot scale [4,6,10].

The Cu/ZnO/Al_2O_3: γ-Al_2O_3 (CZA/γ-Al_2O_3) catalyst system has been broadly investigated and presents high yield and selectivity for CO-rich syngas feed. However, in CO_2-rich conditions, water formation is enhanced due to higher occurrence of Reaction (2) and, at elevated temperature, also of Reaction (3). Since γ-Al_2O_3 is a hydrophilic material, it is subject to competitive adsorption of water in water-rich environments, which deactivates the catalyst by blocking the active sites [11]. The activity of CZA also suffers a negative effect at higher water content, partially because of Al_2O_3 content in its composition. As syngas sources become more diverse, aiming to address environmental motivations, catalysts suitable for CO_2-rich syngas feeds play a deciding role. In comparison to CZA, Cu/ZnO/ZrO_2 (CZZ) presented higher tolerance to water, being more suitable to CO_2-rich syngas hydrogenation [12]. As an alternative to γ-Al_2O_3 for methanol dehydration, the use of zeolites, such as ferrierite (FER), was proposed due to their higher number of acid sites and surface area combined with a high selectivity and slow coke deposition [13–15].

In a previous study [12], we compared CZA and CZZ for direct DME synthesis, in combination with FER. The CZZ/FER system yielded higher DME selectivity and productivity than CZA/FER for all CO_2/CO_X ratios tested. Additionally, we compared the CZZ/FER system to CZZ/γ-Al_2O_3 for direct DME synthesis; the former presented a considerable improvement in DME selectivity and productivity for higher CO_2/CO_X ratios in the inlet gas. Arena *et al.* [16] tested a self-produced CZZ catalyst for an inlet gas composed of CO_2, H_2 and N_2, and an improvement in methanol selectivity was observed in comparison to a commercial CZA catalyst. Catizzone *et al.* [13] tested FER with distinct Si/Al ratios, showing that FER-10 and FER-25 allow higher methanol conversion for the entire temperature range in comparison to γ-Al_2O_3. In the work from Bonura *et al.* [17], hybrid systems combining CuZnZr methanol catalyst and two different zeolites – ferrierite (FER) and mordenite (MOR) – were studied, and the authors observed a greater DME yield using FER. Although these catalytic systems have been studied by different groups, the reaction mechanism is still not well understood.

Kinetic modeling plays a deciding role for scale-up and process optimization of direct DME synthesis at a commercial level. A challenging aspect is the complexity of reaction mechanisms, due to morphological changes in the catalyst surface under varying reaction conditions and multiple reaction pathways, as well as a not completely understood influence of water. For this reason, several models are proposed in literature. Nevertheless, most of them were validated only for the CZA/γ-Al_2O_3 system – an overview is given in Section 2. Additionally, a characteristic of many studies is a limited range for CO_2/CO_X ratios [18]. In our previous work [14], we developed a kinetic model for the CZZ/FER system by combining the methanol synthesis model proposed in [19], originally validated for CZA catalyst, with a rate equation for methanol dehydration based on the mechanism proposed by Arvidsson *et al.* [20]. The parameters were estimated according to 240 experimental points, varying the CO_2/CO_X inlet ratio, temperature, inlet gas flow and the mass of CZZ and FER in the catalyst bed.

The present work addresses two objectives: firstly modeling the direct DME synthesis for a distinct catalytic system – which, to the best of our knowledge, was studied for such process uniquely by our group – and secondly using experimental data for a broad range of operating conditions. In this contribution, we expanded significantly the validation range of the model proposed in [14]. As the experiments from our previous work were carried out at 30 bar, in the present study the pressure was varied between 30 and 54 bar. Moreover, H_2 inlet was varied between 35 and 65% (v/v), which is of interest when fluctuating hydrogen sources are considered as feed component. Also, the CO_2/CO_X ratio was broadened to values as low as 0.12, increasing the robustness of the model. Here, methanol synthesis experiments were additionally performed and included in order to better assess the kinetic regime of the first stage of direct DME synthesis. The resulting new database is combined with the experiments from [14], and the kinetic parameters are estimated for the proposed model.

2. Overview of available models for direct synthesis of DME

Models for direct DME synthesis published in literature are either a combination from methanol synthesis and methanol dehydration rate equations or are directly developed for such process. For methanol synthesis, models differ with respect to the considered adsorption sites, intermediate paths and rate-determining steps, as well as to the choice of global reactions. In the models from Graaf *et al.* [21], Seidel *et al.* [22] and the 1-parameter and 9-parameter models from Campos *et al.* [19], methanol is assumed to be formed both by CO and CO_2 hydrogenation, and (reverse) water–gas shift takes place in parallel. On the other hand, direct CO hydrogenation is neglected in the models developed by Vanden Bussche and Froment [23], Slotboom *et al.* [24], Nestler *et al.* [25] and in the 6-parameter model from Campos *et al.* [19]. As pointed in [24], only two kinetic rate equations are strictly necessary, because the third one is the linear combination of the other two. All aforementioned models were developed for the Cu/ZnO/Al_2O_3 (CZA) catalyst, used industrially for methanol synthesis [26].

Regarding methanol dehydration to DME, Bercic and Levec [27] proposed a model in which a Langmuir–Hinshelwood mechanism with dissociative adsorption of methanol on the catalyst surface is assumed. The formulation includes a denominator where inhibition due to methanol and water adsorption is considered, nevertheless DME adsorption is neglected, as in similar models [14,28,29]. Mollavali *et al.* [28] developed a model based on the mechanism proposed in [29], and, according to their experiments, the rate-determining step is the reaction of a methoxy group with an adsorbed molecule of methanol. These two models were developed for dehydration on γ-Al_2O_3.

In Tables 1 and 2, a summary of kinetic models for direct DME synthesis is displayed. Ng *et al.* [30] and Hadipour and Sohrabi [31]

Table 1
Overview of studies dedicated to kinetic studies of direct DME synthesis.

Work*	Methanol catalyst	DME catalyst	Methanol model	DME model
Ng 1999 [30]	CZA	γ-Al_2O_3	Bussche 1996 [18]	Bercic 1992 [20]
Lu 2004 [29]	CZA	HZSM-5	Self-developed	Self-developed
Aguayo 2007 [32]	CZA	γ-Al_2O_3	Self-developed	Self-developed
Hadipour 2008 [31]	CZA	γ-Al_2O_3	Graaf 1988 [16]	Bercic 1992
Sierra 2010 [33]	CZA	γ-Al_2O_3	Aguayo 2007 [25]	Aguayo 2007
Ereña 2011 [34]	CZA	γ-Al_2O_3	Aguayo 2007	Aguayo 2007
Peláez 2017 [35]	CZA	γ-Al_2O_3	Self-developed[a]	Self-developed[b]
Delgado 2020 [36]	CZA	γ-Al_2O_3	Lu 2004	Lu 2004
Wild 2022 [14]	CZZ	FER	Campos 2021 [15]	Self-developed[c]
This work	CZZ	FER	Campos 2021 [15]	Wild 2022 [14]

*Works and models named by first author and year of publication.
[a] Based on the mechanism published by Vanden Bussche and Froment [23].
[b] Based on the mechanism published by Bercic and Levec [27].
[c] Based on the mechanism published by Arvidsson *et al.* [20].

Table 2
Validation ranges of kinetic models for direct DME synthesis.

Work*	Pressure (bar)	Temperature (°C)	Methanol catalyst mass fraction (%)**	CO_2/CO_X	H_2/CO_X
Ng 1999 [30]	50	250	33–67	0–1	1–4
Lu 2004 [29]	20–40	250–270	80–86	0[b]	0.8–2.1[b]
Aguayo 2007 [32]	10–40	225–325	67	0 or 1	4
Hadipour 2008 [31]	9	230–300	44–58[a]	0.11	1.78
Sierra 2010 [33]	10–40	225–350	67	0	2–4
Ereña 2011 [34]	20–40	225–325	67	0 or 1	2–4
Peláez 2017 [35]	30	250–270	70–92	0–0.29	0.53–1.5
Delgado 2020 [36]	50	220–260	50	0.06–0.43	2.36–2.72
Wild 2022 [14]	30	210–240	50–99	0.4–0.9	1.92–2.12
This work	30–54	200–250	50–99	0.12–0.92	1.44–3.07

*Works and models named by first author and year of publication.
**Mass of methanol catalyst/Total mass of catalyst.
[a] From Delgado *et al.* [18].
[b] CO_2 is reported as reactant in the setup, however, in the experimental results, only CO is mentioned.

combined existing models for methanol synthesis and methanol dehydration rate equations – respectively Vanden Bussche and Froment [23] and Bercic and Levec [27]; and Graaf *et al.* [21] and Bercic and Levec [27] – and re-estimated the parameters for the respective databases.

Lu *et al.* [29] proposed a kinetic model, assuming one active site for methanol synthesis and that DME is formed by the reaction between a methoxy cation with an adsorbed methanol molecule. Aguayo *et al.* [32] proposed three kinetic models of increasing complexity. In the first model, the authors considered CO hydrogenation and water–gas shift reaction (WGSR). In the second one, an inhibition term due to adsorption of water in the catalyst was included. The third model adds CO_2 hydrogenation rate equation. According to their data basis, inhibition by water has a relevant effect in the kinetics, and CO_2 hydrogenation has a low influence in the model. Nevertheless, their experiments were performed with either pure CO or pure CO_2 as carbon source, not taking into account the diversity in mechanisms for distinct mixtures of CO and CO_2. Sierra *et al.* [33] performed experiments with CO and H_2 as feed gases and included a term for deactivation over time in the second model from [32], a phenomenon owed to coke formation. As an improvement to Sierra's model, Ereña *et al.* [34], based on experiments with H_2 + CO or H_2 + CO_2, maintained the deactivation term introduced in [33] and adapted the attenuation term for feeds containing CO_2. Peláez *et al.* [35] developed their own kinetic expressions based on the mechanistic model presented in [23] and on an elementary equation proposed in [27]. The authors aimed to optimize the composition of the catalytic bed, i.e., determine the ideal proportion between the methanol and DME catalysts. In our group, Delgado *et al.* [36] used the model from Lu *et al.* [29], refitted with own experimental data, to optimize CO_x conversion in DME synthesis by varying operating conditions and composition of the catalytic bed, and experimentally validated the simulated results. Also in a work from our group, Wild *et al.* [14] combined the 6-parameter model for methanol synthesis from Campos *et al.* [19] with an additional reaction rate equation for methanol dehydration, derived from density functional theory (DFT) calculations described in [20]. The resulting 8-parameter model was fitted with experimental measurements performed using $Cu/ZnO/ZrO_2$ (CZZ) catalyst for methanol synthesis and H-FER 20 for methanol dehydration, and the result was used to optimize the composition of the catalytic bed for an inlet CO_2/CO_x ratio of 0.9.

3. Experimental study

3.1. Catalyst preparation

The catalyst chosen for the methanol synthesis was a self-produced $Cu/ZnO/ZrO_2$ (CZZ), with a precursor solution of Cu/Zn/Zr: 57/29/14% m/m. The preparation followed a continuous co-precipitation method in a micro jet mixer, where metal nitrate and sodium bicarbonate solutions are mixed at pH 7. The resulting suspension was aged at 40 °C for 2 h. Then, the solids were filtered, dried at 110 °C for 16 h, and calcined at 350 °C for 4 h with a heating ramp of 3 °C·min^{-1}. Further details about the synthesis can be found in [26], and characterization results are presented in [14].

The catalyst chosen for methanol dehydration was the commercial zeolite H-FER-20 (FER), which has a SiO_2/Al_2O_3 ratio of 20. Characterization results for this material can be found in [37]. A calcination with air at 550 °C for 4 h was performed.

Both catalysts were powdered, pressed and sieved into fractions between 250 and 500 μm. The corresponding bulk densities of CZZ and FER were 882.5 and 415.0 kg·m^{-3}, respectively [14].

In order to activate the catalysts, a 300 $mL_N \cdot min^{-1}$ flow containing 5% (v/v) hydrogen in nitrogen was applied, with a temperature increase from 100 to 200 °C at 20 °C·h^{-1}. The temperature of 200 °C was held for one hour and afterwards increased to 240 °C at 12 °C·h^{-1}. Finally, maintaining the temperature at 240 °C, the hydrogen concentration was increased to 50% (v/v), and the flow was held for one hour.

3.2. Experimental setup

Steady-state experiments at various conditions were conducted in a fixed-bed tube reactor made of stainless steel (length: 460 mm, inner diameter: 12 mm) with an inner concentric tube (2 mm) to measure the temperature along the reactor length. Hydrogen (99.999% v/v), carbon monoxide (99.97% v/v), nitrogen (99.9999% v/v), and a mixture of carbon dioxide and nitrogen (50:50 ± 1.0% v/v) (Air Liquide Germany GmbH) were supplied as inlet feed via mass flow controllers (MFCs, Bronkhorst High Tech), regulated using proportional-integral-derivative (PID) control. A flow diagram of the setup is available in our previous publication [38]. The MFCs were calibrated using a flowmeter (Defender 530+, Mesalabs, standard error: 1.0% v/v). The concentration of the reactants (via bypass) and the products were measured via a Fourier transform infrared spectrometer (FTIR, Gasmet CX4000) coupled with a hydrogen analyzer (H_2–/TCD, LFE Conthos 3).

Two experimental series were performed: the first one (Set #1, methanol synthesis) with only CZZ catalyst (3.39 g), and the second one (Set #2, direct DME synthesis) with a mixture containing CZZ (3.39 g) and FER (0.15 g). The latter series corresponds to a CZZ/FER volume composition of 91.5/8.5% v/v, an optimized value determined in our previous work for a CO_2/CO_X ratio of 0.9 [14].

In order to avoid formation of hot spots in the catalytic bed, the catalysts were diluted with 34.9 g of silicon carbide (SiC, Hausen Mineraliengroßhandel GmbH). The catalyst bed was filled as five-fold stacks, to improve the distribution of the components along the reactor, totalizing 200 mm length. The top and the bottom of the reactor were completed with pure SiC. Axial temperature variations in the reactor were lower than 2 °C, therefore isothermal operation was assumed.

The range of operating conditions from our experiments are

summarized in Tables 3 and 4. Previous experiments reported in [14] (here named Set #3) were also included in the experimental database of this work, as CZZ and FER catalysts from the same synthesis batches were used. The experiments performed in this work significantly enlarged the covered operating conditions from our previous work [14] in terms of pressure, temperature, gas hourly space velocity (GHSV), and feed composition. Full experimental data is provided in the Supplementary Information (SI, Section S9).

Our experiments are designed and performed with the aim of capturing mostly the kinetic regime of the reactions, in order to better estimate the parameters related to kinetic rate constants and adsorption of certain compounds. For this reason, our experiments are mostly carried out at high GHSV. We also performed experiments at lower GHSV and lower dilution in N_2, in order to obtain high conversions, providing the kinetic model with information about the behavior of the system under such conditions.

4. Kinetic model development

4.1. Description of the developed model

It is known that the zinc coverage of Cu/Zn-based catalysts varies depending on the operating conditions, i.e., temperature and gas composition [39–41]. Ovesen *et al.* [42] proposed a methodology to estimate the zinc coverage using the Wulf construction, involving the estimation of one parameter. Kuld *et al.* [41] performed DFT calculations and proposed a methodology for the zinc coverage estimation without any extra parameter estimation, which should be valid if the WGSR is close to equilibrium. We tested the approach of Ovesen *et al.* [42] in the model, including an additional parameter. However, this parameter was not statistically significant, and led in our case to a Zn coverage close to unity and almost independent of the gas phase composition. Therefore, it was chosen to neglect the zinc coverage variation in this kinetic model.

Activity decay was observed in the experimental study by measuring reference points. Details about the measurement of such points and the obtained experimental values are given in SI (Section S3). Since the deactivation profile is significantly similar for both methanol and direct DME synthesis experiments, it is probable that only CZZ is losing activity, and FER deactivation is negligible in this period (<600 h). Therefore, a second-order decay model was proposed for CZZ, which is the most commonly used decay rate when sintering is the main deactivation cause [43].

By including a deactivation function, we intend at this moment to describe the system more accurately, consequently increasing the quality of the estimated kinetic parameters. Creation of kinetic models was also tested without the deactivation function, and, although the models are comparable in performance with the ones which include deactivation, we observed that the error had distinct behaviors with variation in time on stream. A more complete analysis and the results for parameter estimation are given in SI (Section S4). In future works we plan to study in more details the deactivation of the catalyst, providing relevant information also for industrial systems. For now, this function should not be extrapolated to an industrial catalyst lifetime, which is typically higher than 20,000 h. First, because it was not validated for such long operating times. Second, industrial processes take place under stable conditions of feed, temperature and pressure, in contrast to laboratorial experiments, where catalyst deactivation is faster due to variable operating conditions.

Table 4
Ranges for feed gas composition (% v/v).

Set	H_2	CO	CO_2	N_2
#1	36.8–60.8	4.6–19.5	2.2–14.9	19.4–44.1
#2	35.2–65.1	3.7–19.1	2.2–16.6	10.0–40.7
#3[a]	41.9–43.4	1.8–12.0	8.6–20.0	35.8–36.9

[a] Experiments from the work of Wild *et al.*[14].

The activity of CZZ catalyst with respect to time on stream ($ToS[h]$) is given by Equation (5):

$$a_{CZZ} = \frac{1}{1 + k_d \cdot (ToS - t_0)} \tag{5}$$

Here, t_0 is the reference time on stream (when $a_{CZZ} = 1$), which was defined at $t_0 = 80\,h$. In the first hours of catalyst operation, deactivation is accelerated due to the rearrangement of the ZnO moieties, influencing the stability of the Cu/ZnO interface [44]. After this period, deactivation becomes moderate, and the behavior of the curve changes. In our case, we observe that the deactivation curve is stable after approximately 80 h, therefore we chose this number as a reference for the deactivation function.

The kinetic approach used in this work is an adapted version of the model described in [14]. The six-parameter model for methanol synthesis proposed in [19] is combined with an additional reaction for methanol dehydration to DME, considering the associative reaction as the rate-determining step [20]. Detailed derivation of the equations can be found in these two articles [14,19], and the elementary steps considered in each are available in SI (Section S7). The reaction rates $\left(r_j\left[mol \cdot kg_{cat}^{-1} \cdot s^{-1}\right]\right)$ for the three reactions considered are given as follows:

$$r_{CO_2 hyd} = a_{CZZ} \cdot k_{CO_2 hyd} \cdot \theta_a \cdot \theta_b \cdot {f_{H_2}}^{1.5} \cdot f_{CO_2} \cdot \left(1 - \frac{f_{CH_3OH} \cdot {f_{H_2O}}}{{f_{H_2}}^3 \cdot f_{CO_2} \cdot {K_{P,CO_2 hyd}}^0}\right) \tag{6}$$

$$r_{rWGS} = a_{CZZ} \cdot k_{rWGS} \cdot \theta_a \cdot \theta_b \cdot f_{CO_2} \cdot f_{H_2O} \cdot \left(1 - \frac{f_{CO} \cdot f_{H_2O}}{f_{H_2} \cdot f_{CO_2} \cdot {K_{P,rWGS}}^0}\right) \tag{7}$$

$$r_{dehyd} = k_{dehyd} \cdot \theta_c \cdot {f_{CH_3OH}}^2 \cdot \left(1 - \frac{f_{DME} \cdot f_{H_2O}}{{f_{CH_3OH}}^2 \cdot {K_{P,dehyd}}^0}\right) \tag{8}$$

The formation of hydrocarbons, especially methane, could occur in this process. However, the amount of methane detected was either zero or close to zero for all measured conditions. Therefore, methane and other hydrocarbons production were neglected in our kinetic model. From our experience with the CZZ/FER system, hydrocarbon production in methanol and direct DME syntheses is more pronounced (although still low) when working without CO_2 in the feed.

In the Equations (6)–(8), k_j correspond to the kinetic constant for each reaction j. Fugacities are given in bar and were calculated using Peng-Robinson cubic equations of state. ${K_{P,CO_2 hyd}}^0\left[bar^{-2}\right]$, ${K_{P,rWGS}}^0[-]$

Table 3
Operating conditions of the experiments.

Set	N° of points	Pressure (bar)	Temperature (°C)	GHSV (s^{-1})	Mass CZZ (g)	Mass FER (g)
#1	194	31–61	190–250	2.17–4.34	3.39	–
#2	381	30–54	200–250	0.79–2.78	3.39	0.15
#3[a]	240	31	210–240	2.78–3.57	1.19–3.59	0.05–1.19

[a] Experiments from the work of Wild *et al.*[14].

and $K_{P,dehyd}{}^{0}[-]$ correspond to the equilibrium constants for each reversible reaction. They were calculated from Gibbs free energy assuming constant heat capacity in the considered temperature range, yielding to three parameters instead of seven. The calculation procedure is described in [38].

$$K_{P,CO_2hyd}{}^{0} = T^{-4.587}\cdot\exp\left(\frac{4698.84}{T}+9.144\right) \tag{9}$$

$$K_{P,rWGS}{}^{0} = T^{-1.097}\cdot\exp\left(-\frac{5331.56}{T}+12.496\right) \tag{10}$$

$$K_{P,dehyd}{}^{0} = T^{1.193}\cdot\exp\left(\frac{3154.77}{T}-10.848\right) \tag{11}$$

Further on, θ_a is the coverage of free Cu/Zn sites for carbon-containing species, θ_b is the coverage of free Cu and Cu/Zn sites for H_2 and H_2O adsorption, and θ_c is the coverage of free zeolite sites, respectively. They are calculated as follows:

$$\theta_a = \left(1+K_1\cdot f_{CO_2}\cdot f_{H_2}{}^{0.5}\right)^{-1} \tag{12}$$

$$\theta_b = \left(1+K_2\cdot f_{H_2O}\cdot f_{H_2}{}^{-0.5}\right)^{-1} \tag{13}$$

$$\theta_c = \left(1+K_3\cdot f_{CH_3OH}\right)^{-1} \tag{14}$$

Here, $K_1\left[bar^{-1.5}\right]$, $K_2\left[bar^{-0.5}\right]$ and $K_3\left[bar^{-1}\right]$ are adsorption constants and need to be estimated. It is important to highlight that methanol dehydration over FER might be limited by mass transfer, due to the intrinsic porosity of the material. Nevertheless, since our experiments were carried out with particles of sizes between 250 and 500 μm, we assumed no mass transfer limitation.

The kinetic constants (k_j) and the adsorption constants (K_j) are usually given as Arrhenius and Van't Hoff equations, respectively [24], i.e.:

$$k_j = A_j\cdot\exp\left(\frac{B_j}{T}\right) = A_j\cdot\exp\left(-\frac{E_{A,j}}{RT}\right) \tag{15}$$

$$K_j = A_j\cdot\exp\left(\frac{B_j}{T}\right) = \exp\left(\frac{\Delta S^{O}{}_{ads,j}}{R}\right)\cdot\exp\left(-\frac{\Delta H^{O}{}_{ads,j}}{RT}\right) \tag{16}$$

The model, as described, contains 13 parameters: two for each kinetic constant k_j, two for each adsorption constant K_j, and the deactivation constant k_d. We tested the model with 13 parameters and found that the activation energy for methanol dehydration $\left(E_{A,dehyd}\right)$ is not statistically significant at the 95% confidence interval. Therefore, we decided to remove this parameter, similarly to other published models [14,35]. Additionally, all B terms for the adsorption constants, i.e., $\Delta H^{0}{}_{ads}$, are statistically equal to 0. This conclusion is consistent with recent publications for methanol synthesis [19,22,24], and, for methanol dehydration, the same approach was followed in [14]. The results for this test are available in SI (Section S5). Therefore, the adsorption term is given here as follows:

$$K_j = \exp\left(\frac{\Delta S^{O}{}_{ads,j}}{R}\right) \tag{17}$$

in which j corresponds to each active site taken into account. As a consequence, the total number of parameters decreased to 9.

4.2. Bussche–Bercic model description

In order to compare the present model to state-of-the-art models published in the literature, we combined the model for methanol synthesis proposed by Vanden Bussche and Froment [23] with the model for methanol dehydration to DME from Bercic and Levec [27]. For a fair comparison, the parameters were refitted utilizing our experimental database. From here on, this model combination will be called Bussche–Bercic. Such combination of models was also employed by Ng *et al.* [30], for example.

The kinetic rate equations from Vanden Bussche and Froment [23] model are:

$$r_{CO_2hyd} = k_{CO_2hyd}\cdot\theta_{BF}{}^{3}\cdot f_{H_2}\cdot f_{CO_2}\cdot\left(1-\frac{f_{CH_3OH}\cdot f_{H_2O}}{f_{H_2}{}^{3}\cdot f_{CO_2}\cdot K_{P,CO_2hyd}{}^{0}}\right) \tag{18}$$

$$r_{rWGS} = k_{rWGS}\cdot\theta_{BF}\cdot f_{CO_2}\cdot\left(1-\frac{f_{CO}\cdot f_{H_2O}}{f_{H_2}\cdot f_{CO_2}\cdot K_{P,rWGS}{}^{0}}\right) \tag{19}$$

$$\theta_{BF} = \left(1+K_1\frac{f_{H_2O}}{f_{H_2}}+K_2\cdot f_{H_2}{}^{0.5}+K_3\cdot f_{H_2O}\right)^{-1} \tag{20}$$

The kinetic rate equation from Bercic and Levec [27] model is:

$$r_{dehyd} = k_{dehyd}\cdot K_4{}^{2}\cdot\theta_{BL}{}^{4}\cdot f_{CH_3OH}{}^{2}\cdot\left(1-\frac{f_{DME}\cdot f_{H_2O}}{f_{CH_3OH}{}^{2}\cdot K_{P,dehyd}{}^{0}}\right) \tag{21}$$

$$\theta_{BL} = \left(1+2\sqrt{K_4\cdot f_{CH_3OH}}+K_5\cdot f_{H_2O}\right)^{-1} \tag{22}$$

where θ_{BF} is the coverage of free sites on the methanol catalyst, and θ_{BL} is the coverage of free sites on the zeolite catalyst.

The form of the equations was adjusted to make them coherent one to the other and comparable to the model we proposed. For both models, reaction rates are given in $[mol\cdot kg_{cat}{}^{-1}\cdot s^{-1}]$. It is important to highlight that, in Bercic and Levec's model [27], the quantity of gas species is given as mole concentration instead of fugacity or partial pressure. However, for isothermal reactors without pressure loss, as considered in this work, these units are equivalent.

Similarly to our model, kinetic rate constants k_j and adsorption constants K_j are lumped parameters from Arrhenius and Van't Hoff equations, respectively. Therefore, the Bussche–Bercic combination contains 16 parameters. If the deactivation constant k_d is included, 17 parameters are involved.

4.3. Reactor equations

In the reactor model, flow was considered one-dimensional and assumed as ideal plug flow (PFR). For each component, the differential equation for material balance with respect to the reactor length is given by:

$$\frac{dy_i}{dz} = \frac{1}{L\dot{N}}\left[m_{CZZ}\cdot\left(\nu_{i,CO_2hyd}\cdot r_{CO_2hyd}+\nu_{i,rWGS}\cdot r_{rWGS}\right)+m_{FER}\cdot\nu_{i,dehyd}\cdot r_{dehyd}\right]-\frac{y_i}{\dot{N}}\cdot\frac{d\dot{N}}{dz} \tag{23}$$

Here, y_i is the molar fraction of component i, z refers to the axial direction, m_{CZZ} and m_{FER} correspond respectively to the total mass of Cu/ZnO/ZrO_2 and H-FER 20 [kg], ν_{ij} is the stoichiometric coefficient of component i in reaction j, and L is the reactor length [m]. $\dot{N}$ is the overall molar flow $\left[mol\cdot s^{-1}\right]$, which changes along the reactor length due to the reduction in the number of moles through CO_2 hydrogenation. The differential equation for the molar flow is:

$$\frac{d\dot{N}}{dz} = -\frac{2\cdot m_{CZZ}\cdot r_{CO_2hyd}}{L} \tag{24}$$

4.4. Parameter estimation

The 815 experimental points were randomly divided into 5 groups of

163 points each, in order to perform a 5-fold cross-validation [45]. The objective of this procedure is the assessment of the model capacity to predict outside its training set, the so-called test error. Points with only CZZ catalyst were equally divided into the groups. In this method, each group of points is removed at a time, and the model is trained for the remaining points. The removed group is used for validation. For each set of training points, the objective function was the minimization of χ^2, which stands for the normalized squared prediction errors of carbon-containing compounds, i.e., CO, CO_2, CH_3OH and DME, as given in Equation (25). For the experiments performed without dehydration catalyst, the term for DME relative error was not considered.

$$\chi^2 = \sum_{i=1}^{N_P} \frac{\left(y^i_{CO,out} - \widehat{y}^i_{CO,out}\right)^2}{{y^i_{CO,out}}^2} + \frac{\left(y^i_{CO_2,out} - \widehat{y}^i_{CO_2,out}\right)^2}{{y^i_{CO_2,out}}^2} + \frac{\left(y^i_{CH_3OH,out} - \widehat{y}^i_{CH_3OH,out}\right)^2}{{y^i_{CH_3OH,out}}^2} + \sum_{i=1}^{N^*_P} \frac{\left(y^i_{DME,out} - \widehat{y}^i_{DME,out}\right)^2}{{y^i_{DME,out}}^2} \quad (25)$$

N_P corresponds to the total number of points in the training sets, and N^*_P refers to the points for the CZZ:FER system. $y^i_{j,out}$ is the experimental output molar fraction of gas j in experiment i, and $\widehat{y}^i_{j,out}$ is the simulated output molar fraction of gas j in experiment i.

The described model has 9 parameters, namely: k_{CO_2hyd} (A and B), k_{rWGS} (A and B), k_{dehyd} (A), K_1, K_2, K_3 and k_d. To improve numerical sensitivity due to parameters with distinct greatness orders, in this work the three A terms in the kinetic constants were estimated in the logarithmic form, i.e., $a = \ln A \therefore A = \exp(a)$.

The cross validation, i.e., k-fold CV is calculated as given below [45]:

$$CV_{(k)} = \frac{1}{k}\sum_{i=1}^{k} {\chi^2}_i \quad (26)$$

In this study, $k = 5$, since a 5-fold cross-validation was performed.

The confidence interval (CI) for each parameter was calculated based on the standard deviation of the estimations for the five groups, assuming Student's t-distribution with four degrees of freedom.

$$CI(1-\alpha) = \frac{s \cdot t_{\alpha/2,k-1}}{\sqrt{k}} \quad (27)$$

Here, α is the significance level, chosen to be 0.05 in this study, s is the sample's standard deviation, k is the sample size, and $t_{\alpha/2,k-1}$ is the Student's two-tailed t-distribution value for a significance level of α and $k-1$ degrees of freedom.

The normalized mean squared error and the mean relative error for a component j were calculated according to the following formulae:

$$MSE_{normj} = \frac{1}{N_P}\sum_{i=1}^{N_P} \frac{\left(y^i_{j,out} - \widehat{y}^i_{j,out}\right)^2}{{y^i_{j,out}}^2} \quad (28)$$

$$MRE_j = \frac{1}{N_P}\sum_{i=1}^{N_P} \frac{\left|y^i_{j,out} - \widehat{y}^i_{j,out}\right|}{y^i_{j,out}} \quad (29)$$

All calculations were performed in Matlab R2021b. Molar fractions and molar flow – Equations (23) and (24) – were integrated using the *ode45* function, with absolute and relative tolerances set to 10^{-8}. Minimization of χ^2 was performed using the built-in *fminsearch* function. Tolerance of X was set to 10^{-4}, and the function tolerance was set to 10^{-6}. Due to the denominators in Equations (6)–(8), (12)–(14) and (18)–(22), initial molar fractions for all components were set as at least $1{\cdot}10^{-7}$ (0.1 ppm), to avoid numerical indetermination in the reactor inlet. Different initial guesses were tested, in order to find multiple local minima and to choose the lowest objective function among them.

5. Results

5.1. Parameter estimation

The kinetic model was successfully developed. The estimated parameters and the 95% confidence interval for the training set with the lowest overall χ^2 value are given in Table 5. The χ^2 for the chosen training set is equal to 25.107, and the $CV_{(5)}$ for this model is equal to 25.123, substantially lower than $\chi^2 = 41.099$ and $CV_{(5)} = 41.137$, obtained with the Bussche–Bercic model. Results for all sets from both models are available in SI (Section S1). For both models, the lowest χ^2 is close to their respective $CV_{(5)}$, indicating the ability of the models to predict results outside the training set. The 95% confidence intervals (CI) shown in the table for all parameters confirm their statistical relevance.

The normalized mean squared error and the mean relative error for the carbon-containing compounds, i.e., CO, CO_2, methanol and DME, are given in Table 6. The models are overall comparable in performance with respect to CO and CO_2. For methanol synthesis (Set #1), Bussche–Bercic slightly outperforms the present model for CO and CO_2, and our model is slightly better for methanol. For direct DME synthesis (Sets #2 and #3), the present model outperforms Bussche–Bercic for all substances but CO_2. Furthermore, the mean relative error for the DME prediction in our model is below 10%, which is a good indicator of its quality.

Parity plots for the carbon-containing compounds are presented in Fig. 1, with the points being distinguished according to the experimental sets presented in Tables 3 and 4. Simulations for CO (Fig. 1a) and CO_2 (Fig. 1b) are in good agreement with the experiments, with 99% of the CO points and all of CO_2 points within the 20% range.

Within the CZZ/FER system (Sets #2 and #3 combined), 554 of the 621 methanol points (89%) are within the 20% lines, and deviations are well-distributed. For the CZZ system (Set #1), 145 of the 194 methanol points (75%) are inside the 20% lines (Fig. 1c). A slight underestimation trend is observed for higher methanol concentration in the CZZ experiments. While this phenomenon probably occurs because most methanol points used for the parameter estimation are concentrated at low values (<0.75% v/v), it is not an issue here, since the focus of this model is to simulate the direct DME synthesis, in which methanol concentration is always low.

Regarding DME (Fig. 1d), 588 of the 621 data points are within the 20% range, which corresponds to 95% of the points. As can be seen in the figure, the present model is particularly good in predicting high DME yields (>3% volume fraction), showing the reliability of the model also for high yield conditions. Another aspect of our work is the expansion of the validation range for DME output. While Set #3 covers DME yields up to 1.07% v/v, in Set #2 a volume fraction of nearly 6% v/v is reached (corresponding to a CO_X conversion of 51%). Nevertheless, the new model comprises most points of Set #3 in the 20% range – only five out of 240 points are underestimated. Using the refitted Bussche–Bercic model, only 79% of the points for DME yield are located within the 20% limit. Parity plots for this combination are available in the SI (Section S2).

5.2. Comparison between experiments and simulations

A meaningful kinetic model needs to exhibit appropriate sensitiveness to the input variables, which in this case are: temperature, pressure, inlet composition and space velocity. Such characteristic is more efficiently achieved the wider the training range is. The new experiments for direct DME synthesis (Set #2) permit, for example, a more precise evaluation of the effect of inlet gas composition and overall pressure. In Set #2, the pressure range was expanded up to 54 bar, and the hydrogen concentration was varied between 35 and 65% (v/v). Such variations are important in order to simulate experiments using syngas from

Table 5
Estimated parameters within the chosen training set.

Parameter		Value ± 95% CI		Unit
k_{CO_2hyd}	$\ln A$	15.34 ± 0.21	$k_{CO_2hyd} = 4.573 \cdot 10^{6} \cdot \exp\left(-\frac{98350}{RT}\right)$	$mol \cdot s^{-1} \cdot kg_{cat}^{-1} \cdot bar^{-2.5}$
	B	$(-11.829 \pm 0.082) \cdot 10^{3}$		
k_{rWGS}	$\ln A$	39.26 ± 0.65	$k_{rWGS} = 1.121 \cdot 10^{17} \cdot \exp\left(-\frac{177000}{RT}\right)$	$mol \cdot s^{-1} \cdot kg_{cat}^{-1} \cdot bar^{-2}$
	B	$(-21.29 \pm 0.33) \cdot 10^{3}$		
k_{dehyd}	$\ln A$	3.72 ± 0.15	$k_{dehyd} = 41.1$	$mol \cdot s^{-1} \cdot kg_{cat}^{-1} \cdot bar^{-2}$
K_1	A	0.449 ± 0.035	$K_1 = 0.449$	$bar^{-1.5}$
K_2	A	46.2 ± 2.3	$K_2 = 46.2$	$bar^{-0.5}$
K_3	A	116 ± 17	$K_3 = 116$	bar^{-1}
k_d		$(9.70 \pm 0.36) \cdot 10^{-4}$	$k_d = 9.70 \cdot 10^{-4}$	h^{-1}

*R in $J.mol^{-1}.K^{-1}$.

Table 6
Statistical indicators of the models' performance.

		Present model			Bussche–Bercic		
		All points	CZZ (Set #1)	CZZ + FER (Sets #2, #3)	All points	CZZ (Set #1)	CZZ + FER (Sets #2, #3)
χ^2		25.11	5.482	19.63	41.10	5.099	36.00
$MSE_{norm} \cdot 10^3$	CO	2.191	0.871	2.604	3.990	0.598	5.050
	CO_2	1.727	2.811	1.389	1.092	0.975	1.129
	CH_3OH	17.72	24.57	15.57	21.31	24.71	20.25
	DME	12.04	–	12.04	31.54	–	31.54
$MRE \cdot 10^2$	CO	2.950	2.292	3.155	3.158	1.821	3.576
	CO_2	3.163	4.161	2.851	2.309	2.408	2.278
	CH_3OH	10.55	12.44	9.956	11.82	12.64	11.56
	DME	8.888	–	8.888	13.36	–	13.36

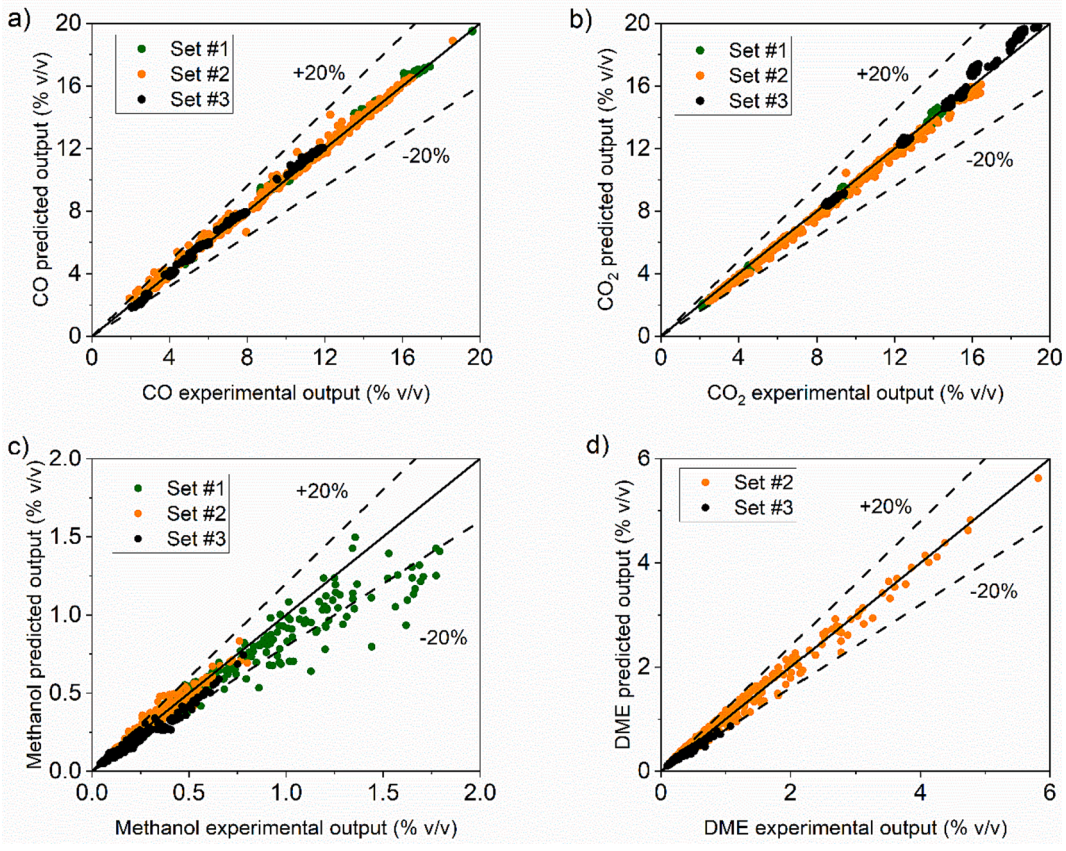

Fig. 1. Parity plots of (a) CO, (b) CO_2, (c) methanol and (d) DME outlet concentration (% v/v). Set #1: methanol synthesis experiments; Set #2: direct DME synthesis experiments from this work; Set #3: direct DME synthesis experiments from Wild et al. [14].

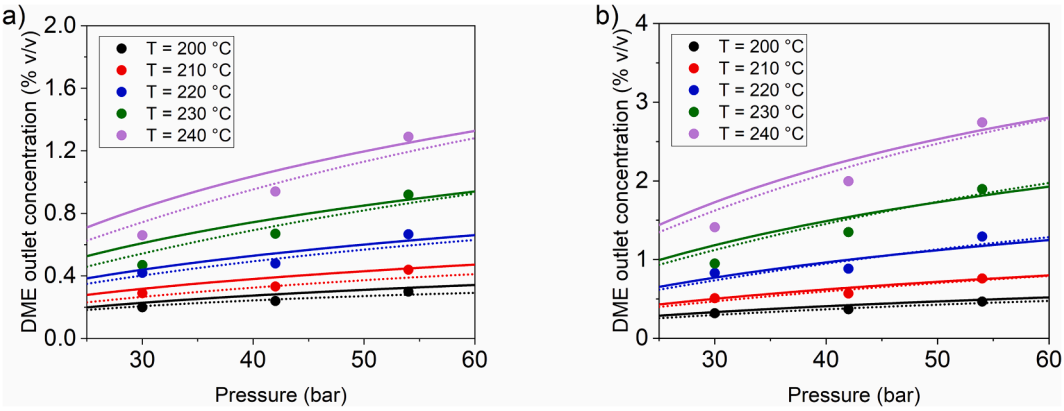

Fig. 2. Comparison between experimental and predicted DME output values for the following conditions: $m_{CZZ} = 3.392\,g$, $m_{FER} = 0.148\,g$, (a) $H_2/CO/CO_2/N_2$ (feed) = 0.4513/0.0769/0.1210/0.3508, $GHSV = 1.984\,s^{-1}$; (b) $H_2/CO/CO_2/N_2$ (feed) = 0.4528/0.1157/0.0795/0.3520, $GHSV = 1.190\,s^{-1}$. Solid lines refer to the present model, and dotted lines, to Bussche–Bercic.

multiple sources, which do not necessarily contain the stoichiometric quantity of H_2 and CO_X.

In Fig. 2, experimental and simulated data for distinct pressures and temperatures are shown. As the experiments were performed at different times on stream, a single ToS value was employed to build the simulation curves, namely the average time for the experiments with both CZZ and FER catalysts (Sets #2 and #3): 216.5 h. This value corresponds to an activity coefficient of 0.8830 in this model and 0.8516 in the Bussche–Bercic model.

From the simulations, it can be observed that both models are in good agreement with the experimental data and follow the expected trend, namely an increase in DME output for higher pressures. Fig. 2a and 2b distinguish themselves with respect to CO_2/CO_X ratio and space velocity; nevertheless, the performance is similar in both of them, which highlights the flexibility of the model.

Equilibrium lines are shown in the plots as dashed-dotted lines. When the reactor simulation curves were far from the equilibrium lines – as in Fig. 2 –, the latter were not shown in the graph, but were made available in the SI (Section S6). This was done to improve clarity of the plots.

In Fig. 3a, experimental and simulated values for DME output concentration are shown as a function of temperature, pressure and GHSV. Both models accurately describe the overall behavior of the points. For temperatures above 250 °C, the slope decreases for all values of pressure, as the system approaches thermodynamic equilibrium – shown by the dashed-dotted lines. The decrease in slope occurs for temperature values above the experimental range, highlighting the potential of the model for extrapolation, since thermodynamic consistency is ensured by the equations. For inlet gas with less H_2 and more inert (Fig. 3b), the present model accurately predicts the experiments, with a slight overestimation. Since conversion is expressively lower than equilibrium, no decay in slope can be observed at the considered temperature range. For Bussche–Bercic, the tendency is well captured; however, overestimation is quite significant, which is discussed in more details in Fig. 5 for varied H_2 contents.

In Fig. 4, the sensitivity of the models with respect to CO_2/CO_X ratio is displayed. The present model exhibits an outstanding agreement with the experimental points for CO_2-rich inlet feeds, while Bussche–Bercic tends to underestimate the results for DME outlet concentration in such conditions. The simulated curves are closer to equilibrium as the CO_2/CO_X inlet ratio increases. From a quantitative perspective, the approach to equilibrium, η, was estimated according to Equation (30) [46]:

$$\eta_j = \frac{\prod_{products} f_i^{\nu_i}}{\prod_{reactants} f_i^{\nu_i}} \cdot \frac{1}{K_{P,j}{}^0} \tag{30}$$

For a temperature of 250 °C and a pressure of 30 bar – the condition with higher proximity to equilibrium in Fig. 4 –, we have performed calculations of η for the three reactions. The results are available in SI (Section S8). A wide range of η is observed for the three reactions, demonstrating the robustness of the model for different conversion levels, including close to equilibrium.

In Fig. 5, experimental and simulated values for DME output

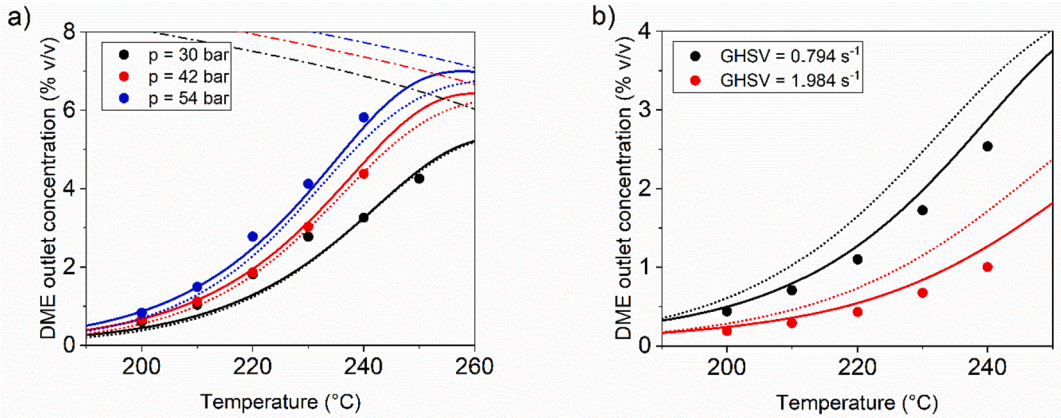

Fig. 3. Comparison between experimental and predicted DME output values for the following conditions: $m_{CZZ} = 3.392\,g$, $m_{FER} = 0.148\,g$, (a) $H_2/CO/CO_2/N_2$ (feed) = 0.4552/0.1682/0.0225/0.3541, $GHSV = 0.794\,s^{-1}$, (b) $H_2/CO/CO_2/N_2$ (feed) = 0.3531/0.1427/0.1007/0.4035, p = 42 bar. Solid lines refer to the present model; dotted lines, to Bussche–Bercic, and dashed-dotted lines, to the equilibrium.

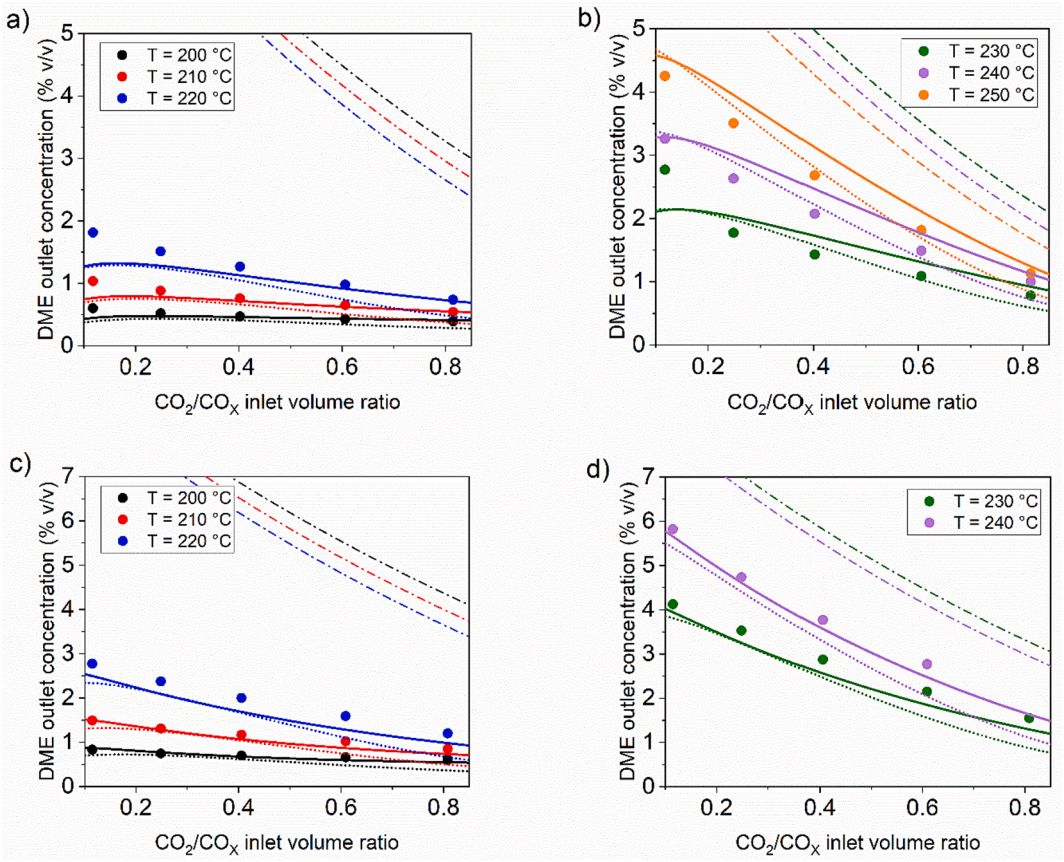

Fig. 4. Comparison between experimental and predicted DME output values for the following conditions: $m_{CZZ} = 3.392\,g$, $m_{FER} = 0.148\,g$, $GHSV = 0.794\,s^{-1}$, (a,b) $H_2/CO_X/N_2$ (feed) = 0.4521/0.1963/0.3516, p = 30 bar; (c,d) $H_2/CO_X/N_2$ (feed) = 0.4529/0.1948/0.3523, p = 54 bar. Solid lines refer to the present model; dotted lines, to Bussche–Bercic, and dashed-dotted lines, to the equilibrium.

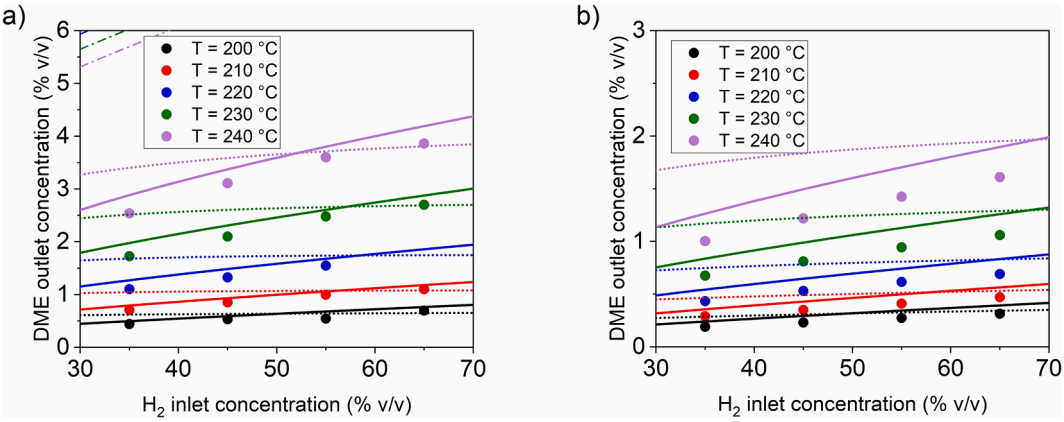

Fig. 5. Comparison between experimental and predicted DME output values for the following conditions: $CO/CO_2/N_2$ (feed) = 0.1452/0.1029/balance, $m_{CZZ} = 3.392\,g$, $m_{FER} = 0.148\,g$, $p = 42\,bar$, (a) $GHSV = 0.794\,s^{-1}$, (b) $GHSV = 1.984\,s^{-1}$. Solid lines refer to the present model; dotted lines, to Bussche–Bercic, and dashed-dotted lines, to the equilibrium.

concentration are shown as functions of H_2 inlet concentration. For both GHSV values (Fig. 5a and 5b), the model introduced in this work is able to capture the behavior of experimental data, namely a steep increase in DME yield for higher H_2 inlet concentrations. On the other hand, the Bussche–Bercic model is less sensitive to such parameter, as can be observed in the behavior of the curves, almost linear with respect to hydrogen inlet molar fraction. Comparing the two reaction rate equations for CO_2 hydrogenation (Eqs. (6) and (18)), one can observe the difference in the exponents of f_{H_2}: 1.5 for the present model and 1 for Bussche–Bercic, showing that the apparent order of H_2 in the present model helps to simulate more adequately the experimental system. The equation is based on theoretical studies in which formic acid hydrogenation is considered as the rate-determining step of methanol synthesis [38]. In other recent models, the exponent of f_{H_2} is also greater than 1: in [22], the exponent is 2, and in the 6-parameter model from [24] the exponent is 1.5, as in this work.

In conclusion, the reason why our model outperforms Bussche–Bercic could be attributed to the following factors: (i) the model proposed by Vanden Bussche and Froment [23] for methanol synthesis assumes a single site for CO_2 and H_2 adsorption. This assumption is altered even in

recent models based on their work, such as Slotboom *et al.* [24], which considers three active sites; (ii) the model of Vanden Bussche and Froment [23] considers hydrogen to have an apparent order of 1, while our model considers it 1.5, the latter being in much better agreement with the experiments (see Fig. 5); (iii) with respect to the model for methanol dehydration proposed by Bercic and Levec [27], the authors assume a dissociative adsorption of methanol, and, in the present contribution, the associative mechanism is assumed to be dominant. As discussed in [20], the associative mechanism prevails for reaction temperatures below 300 °C carried out with zeolites, consistent with the validation range of our model.

5.3. Industrial conditions

Using our model, we performed simulations under conditions closer to industrial operation, namely pressure equal to 60 bar and inlet gas without N_2 dilution, with a composition of 70% H_2, 12% CO and 18% CO_2. The results for DME outlet concentration as a function of the normalized reactor length are shown in Fig. 6. For a GHSV equal to 0.05 s^{-1} (Fig. 6a), it can be seen that, at 240 °C, the equilibrium conversion is already approached at about 40% of the reactor length. Fig. 6a also shows that experiments carried out at 220 °C or 230 °C would result in similar outlet DME concentration, since the reaction slows down earlier at 230 °C. These analyses highlight the relevance of kinetic models under industrial conditions, as they can be used, for example, to calculate the required catalyst mass to reach thermodynamic equilibrium, thus optimizing the use of resources. In Fig. 6b, simulations have been carried out for a GHSV equal to 0.1 s^{-1}. As expected, the kinetic regime takes place in a longer length than in the other simulation; however, it is already possible to see the influence of the thermodynamic limitation at higher temperatures.

Kinetic models are fundamental for reactor design and techno-economic analysis. For example, Campos *et al.* [47], in our group, used the 6p model for methanol synthesis [19] to propose a plant with intermediate condensation steps and compared it with the usual one-step process. The authors concluded that the implementation of reactors in series leads to higher CO_2 conversion and lower net production costs. Semmel *et al.* [48] used a kinetic model for liquid phase DME synthesis to perform a techno-economic analysis of different approaches to this process. Kinetic models are also useful at the laboratory scale to predict experimental results based on desired inlet conditions and available resources, thus aiding in experimental design.

As mentioned in the Section 3, our experiments were performed under conditions that allow a better estimation of the kinetic parameters, reducing effects such as hot spots and mass transfer limitation. In large scale reactors, these effects have to be taken into account by coupling the kinetic rate equations with a heat transfer model and a gas diffusion model within the catalyst pellets. Another aspect to consider is catalyst deactivation. In our model, we have included a deactivation function compatible with sintering; however, enhanced deactivation due to prolonged exposure to high water content may occur for CO_2-rich feeds [49,50] and requires further investigation.

6. Conclusions

A kinetic model for direct DME synthesis on the CZZ/FER catalyst system was successfully developed and validated for relevant industrial conditions of temperature and pressure. The experiments comprise a broad range of CO_2/CO_X ratio and H_2 inlet fraction, addressing the current necessity of sustainable methanol production, especially with respect to hydrogen produced via electrolysis supplied by solar or wind power. A published database was combined with new experiments for methanol and for direct DME synthesis, resulting in 815 steady-state points, which is, to the best of our knowledge, the broadest one published in open literature for this catalytic system. As a contribution to other scientists in this field, this work provides a timely overview of the models available for the direct DME synthesis and an extensive database used in the model validation, which is available in the supplementary information.

The present model adequately simulates the direct DME synthesis at both low- and high-conversion regions, and presents proper sensitiveness to variations in pressure, temperature, inlet H_2 concentration and CO_2/CO_X inlet ratio. For comparison, we refitted a combination of two state-of-the-art models for methanol synthesis and methanol dehydration to DME with our experimental data. Our new model has 5 significant parameters less than the one derived from open literature and outperforms the latter, especially for variations in H_2 inlet molar fraction.

Such a widely validated kinetic model is suitable to be used for scale-up, techno-economic analyses and optimization of reactor design, allowing for an industrial application of direct DME synthesis with multiple conditions. A second-order deactivation function for the CZZ catalyst was also included in the model. However, extrapolations to industrial process conditions, especially related to the loss of catalyst activity at higher times on stream due to prolonged exposure to water, require additional validation. Such topic is the subject of current investigations in our group.

CRediT authorship contribution statement

Gabriela Rodrigues Niquini: Conceptualization, Methodology, Formal analysis, Visualization, Writing – original draft, Writing – review & editing. **Bruno Lacerda de Oliveira Campos:** Investigation, Methodology, Writing – original draft, Writing – review & editing. **Karla**

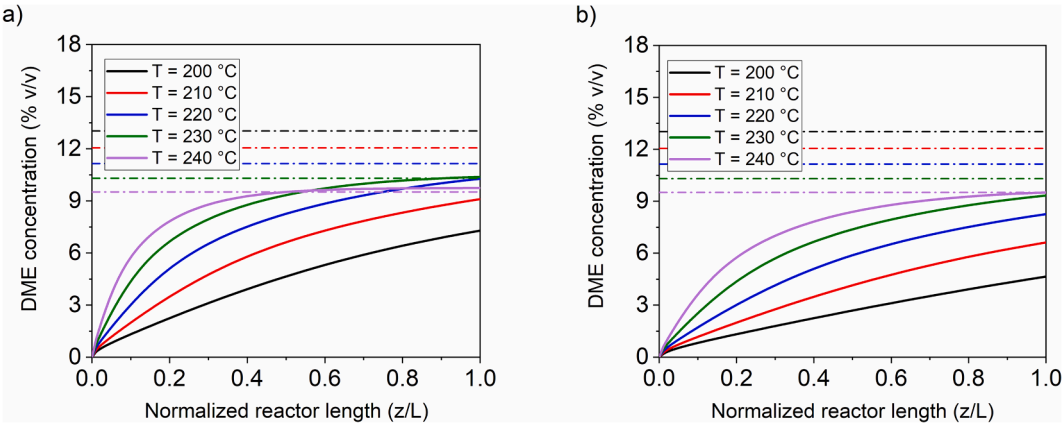

Fig. 6. Simulated DME concentration with respect to normalized reactor length at the following conditions: inlet gas composition = 70% H_2, 12% CO and 18% CO_2; p = 60 bar; CZZ:FER = 91.5:8.5 (v/v). (a) GHSV = 0.05 s^{-1}; (b) GHSV = 0.1 s^{-1}. Solid lines refer to simulated values, dashed-dotted lines refer to equilibrium.

Herrera Delgado: Conceptualization, Funding acquisition, Project administration, Supervision, Writing – original draft, Writing – review & editing. **Stephan Pitter:** Funding acquisition, Project administration, Supervision, Writing – original draft, Writing – review & editing. **Jörg Sauer:** Funding acquisition, Methodology, Project administration, Supervision, Writing – original draft, Writing – review & editing.

Declaration of competing interest

The authors declare that they have no known competing financial interests or personal relationships that could have appeared to influence the work reported in this paper.

Data availability

Experimental data is available in the supplementary information.

Acknowledgements

We acknowledge the Helmholtz Association for funding this research (Research Programme “Storage and Cross-linked Infrastructures”, Topic “Synthetic Hydrocarbons”, number 380302). We thank the Federal Ministry of Economic Affairs and Climate Action from Germany (BMWK) for funding this research through the 3D-Process project (project no. 03EN2065E). We also thank the Coordenação de Aperfeiçoamento de Pessoal de Nível Superior (CAPES) for financing the PhD scholarship of Bruno Lacerda de Oliveira Campos (Process Number: 88881.174609/2018-01). We kindly acknowledge the support of TVT-KIT group, analytics and chemical laboratory colleagues.

Appendix A. Supplementary data

Supplementary data to this article can be found online at https://doi.org/10.1016/j.cej.2023.147968.

References

[1] A. Hofrichter, D. Rank, M. Heberl, M. Sterner, Determination of the optimal power ratio between electrolysis and renewable energy to investigate the effects on the hydrogen production costs, Int. J. Hydrogen Energy 48 (5) (2023) 1651–1663, https://doi.org/10.1016/j.ijhydene.2022.09.263.
[2] T. Amirthan, M.S.A. Perera, The role of storage systems in hydrogen economy: a review, J. Nat. Gas Sci. Eng. 108 (2022), https://doi.org/10.1016/j.jngse.2022.104843.
[3] M. van der Spek, C. Banet, C. Bauer, P. Gabrielli, W. Goldthorpe, M. Mazzotti, S. T. Munkejord, N.A. Røkke, N. Shah, N. Sunny, D. Sutter, J.M. Trusler, M. Gazzani, Perspective on the hydrogen economy as a pathway to reach net-zero CO2emissions in Europe, Energ. Environ. Sci. 15 (3) (2022) 1034–1077, https://doi.org/10.1039/d1ee02118d.
[4] S. Banivaheb, S. Pitter, K.H. Delgado, M. Rubin, J. Sauer, R. Dittmeyer, Recent progress in direct DME synthesis and potential of bifunctional catalysts, Chem. Ing. Tech. 94 (3) (2022) 240–255, https://doi.org/10.1002/cite.202100167.
[5] K. Saravanan, H. Ham, N. Tsubaki, J.W. Bae, Recent progress for direct synthesis of dimethyl ether from syngas on the heterogeneous bifunctional hybrid catalysts, Appl Catal B 217 (2017) 494–522, https://doi.org/10.1016/j.apcatb.2017.05.085.
[6] N. Dahmen, U. Arnold, N. Djordjevic, T. Henrich, T. Kolb, H. Leibold, J. Sauer, High pressure in synthetic fuels production, J. Supercrit. Fluids 96 (2015) 124–132, https://doi.org/10.1016/j.supflu.2014.09.031.
[7] B.V. Ga, P.Q. Thai, Soot emission reduction in a biogas-DME hybrid dual-fuel engine, Appl. Sci. 10 (10) (2020), https://doi.org/10.3390/app10103416.
[8] M. Drexler, P. Haltenort, U. Arnold, J. Sauer, S.A. Karakoulia, K.S. Triantafyllidis, Progress in the anhydrous production of oxymethylene ethers (OME) as a renewable diesel fuel in a liquid phase process, Catal. Today (2022), https://doi.org/10.1016/j.cattod.2022.07.015.
[9] Z. Azizi, M. Rezaeimanesh, T. Tohidian, M.R. Rahimpour, Dimethyl ether: a review of technologies and production challenges, Chem. Eng. Process: Process Intensif. 82 (2014) 150–172, https://doi.org/10.1016/j.cep.2014.06.007.
[10] V. Dieterich, A. Buttler, A. Hanel, H. Spliethoff, S. Fendt, Power-to-liquid via synthesis of methanol, DME or Fischer–Tropsch-fuels: a review, Energ. Environ. Sci. 13 (10) (2020) 3207–3252, https://doi.org/10.1039/d0ee01187h.
[11] S. Sahebdelfar, P.M. Bijani, F. Yaripour, Deactivation kinetics of γ-Al2O3 catalyst in methanol dehydration to dimethyl ether, Fuel 310 (2022), https://doi.org/10.1016/j.fuel.2021.122443.
[12] S. Wild, S. Polierer, T.A. Zevaco, D. Guse, M. Kind, S. Pitter, K. Herrera Delgado, J. Sauer, Direct DME synthesis on CZZ/H-FER from variable CO(2)/CO syngas feeds, RSC Adv 11(5) (2021) 2556-2564. https://doi.org/10.1039/d0ra09754c.
[13] E. Catizzone, M. Migliori, A. Purita, G. Giordano, Ferrierite vs. γ-Al2O3: The superiority of zeolites in terms of water-resistance in vapour-phase dehydration of methanol to dimethyl ether, J. Energy Chem. 30 (2019) 162–169, https://doi.org/10.1016/j.jechem.2018.05.004.
[14] S. Wild, B. Lacerda de Oliveira Campos, T.A. Zevaco, D. Guse, M. Kind, S. Pitter, K. Herrera Delgado, J. Sauer, Experimental investigations and model-based optimization of CZZ/H-FER 20 bed compositions for the direct synthesis of DME from CO2-rich syngas, Reaction Chemistry & Engineering 7(4) (2022) 943-956. https://doi.org/10.1039/d1re00470k.
[15] E. Catizzone, G. Bonura, M. Migliori, F. Frusteri, G. Giordano, CO(2) recycling to dimethyl ether: state-of-the-art and perspectives, Molecules 23 (1) (2017), https://doi.org/10.3390/molecules23010031.
[16] F. Arena, K. Barbera, G. Italiano, G. Bonura, L. Spadaro, F. Frusteri, Synthesis, characterization and activity pattern of Cu–ZnO/ZrO2 catalysts in the hydrogenation of carbon dioxide to methanol, J. Catal. 249 (2) (2007) 185–194, https://doi.org/10.1016/j.jcat.2007.04.003.
[17] G. Bonura, F. Frusteri, C. Cannilla, G. Drago Ferrante, A. Aloise, E. Catizzone, M. Migliori, G. Giordano, Catalytic features of CuZnZr–zeolite hybrid systems for the direct CO2-to-DME hydrogenation reaction, Catalysis Today 277 (2016) 48–54, https://doi.org/10.1016/j.cattod.2016.02.013.
[18] N. Delgado Otalvaro, P.G. Bilir, K. Herrera Delgado, S. Pitter, J. Sauer, Kinetics of the direct DME synthesis: state of the art and comprehensive comparison of semi-mechanistic, data-based and hybrid modeling approaches, Catalysts 12 (3) (2022), https://doi.org/10.3390/catal12030347.
[19] B. Lacerda de Oliveira Campos, K. Herrera Delgado, S. Pitter, J. Sauer, Development of Consistent Kinetic Models Derived from a Microkinetic Model of the Methanol Synthesis, Industrial & Engineering Chemistry Research 60(42) (2021) 15074-15086. https://doi.org/10.1021/acs.iecr.1c02952.
[20] A.A. Arvidsson, P.N. Plessow, F. Studt, A. Hellman, Influence of acidity on the methanol-to-DME reaction in zeotypes: a first principles-based microkinetic study, J. Phys. Chem. C 124 (27) (2020) 14658–14663, https://doi.org/10.1021/acs.jpcc.0c03125.
[21] G.H. Graaf, E.J. Stamhuis, A.A.C.M. Beenackers, Kinetics of low-pressure methanol synthesis, Chem. Eng. Sci. 43 (12) (1988) 3185–3195, https://doi.org/10.1016/0009-2509(88)85127-3.
[22] C. Seidel, A. Jörke, B. Vollbrecht, A. Seidel-Morgenstern, A. Kienle, Kinetic modeling of methanol synthesis from renewable resources, Chem. Eng. Sci. 175 (2018) 130–138, https://doi.org/10.1016/j.ces.2017.09.043.
[23] K.M.V. Bussche, G.F. Froment, A steady-state kinetic model for methanol synthesis and the water gas shift reaction on a commercial Cu/ZnO/Al2O3Catalyst, J. Catal. 161 (1) (1996) 1–10, https://doi.org/10.1006/jcat.1996.0156.
[24] Y. Slotboom, M.J. Bos, J. Pieper, V. Vrieswijk, B. Likozar, S.R.A. Kersten, D.W. F. Brilman, Critical assessment of steady-state kinetic models for the synthesis of methanol over an industrial Cu/ZnO/Al2O3 catalyst, Chem. Eng. J. 389 (2020), https://doi.org/10.1016/j.cej.2020.124181.
[25] F. Nestler, A.R. Schütze, M. Ouda, M.J. Hadrich, A. Schaadt, S. Bajohr, T. Kolb, Kinetic modelling of methanol synthesis over commercial catalysts: a critical assessment, Chem. Eng. J. 394 (2020), https://doi.org/10.1016/j.cej.2020.124881.
[26] S. Polierer, D. Guse, S. Wild, K. Herrera Delgado, T.N. Otto, T.A. Zevaco, M. Kind, J. Sauer, F. Studt, S. Pitter, Enhanced direct dimethyl ether synthesis from CO2-rich syngas with Cu/ZnO/ZrO2 catalysts prepared by continuous co-precipitation, Catalysts 10 (8) (2020), https://doi.org/10.3390/catal10080816.
[27] G. Bercic, J. Levec, Intrinsic and global reaction rate of methanol dehydration over .gamma.-alumina pellets, Industrial & Engineering Chemistry Research 31(4) (1992) 1035-1040. https://doi.org/10.1021/ie00004a010.
[28] M. Mollavali, F. Yaripour, H. Atashi, S. Sahebdelfar, Intrinsic kinetics study of dimethyl ether synthesis from methanol on γ-al2o3 catalysts, Ind. Eng. Chem. Res. 47 (9) (2008) 3265–3273, https://doi.org/10.1021/ie800051h.
[29] W.-Z. Lu, L.-H. Teng, W.-D. Xiao, Simulation and experiment study of dimethyl ether synthesis from syngas in a fluidized-bed reactor, Chem. Eng. Sci. 59 (22–23) (2004) 5455–5464, https://doi.org/10.1016/j.ces.2004.07.031.
[30] K.L. Ng, D. Chadwick, B.A. Toseland, Kinetics and modelling of dimethyl ether synthesis from synthesis gas, Chem. Eng. Sci. 54 (15–16) (1999) 3587–3592, https://doi.org/10.1016/s0009-2509(98)00514-4.
[31] A. Hadipour, M. Sohrabi, Synthesis of some bifunctional catalysts and determination of kinetic parameters for direct conversion of syngas to dimethyl ether, Chem. Eng. J. 137 (2) (2008) 294–301, https://doi.org/10.1016/j.cej.2007.04.039.
[32] A.T. Aguayo, J. Ereña, D. Mier, J.M. Arandes, M. Olazar, J. Bilbao, Kinetic modeling of dimethyl ether synthesis in a single step on a CuO−ZnO−Al2O3/γ-Al2O3 Catalyst, Ind. Eng. Chem. Res. 46 (17) (2007) 5522–5530, https://doi.org/10.1021/ie070269s.
[33] I. Sierra, J. Ereña, A.T. Aguayo, M. Olazar, J. Bilbao, Deactivation kinetics for direct dimethyl ether synthesis on a CuO−ZnO−Al2O3/γ-Al2O3 Catalyst, Ind. Eng. Chem. Res. 49 (2) (2010) 481–489, https://doi.org/10.1021/ie900978a.
[34] J. Ereña, I. Sierra, A.T. Aguayo, A. Ateka, M. Olazar, J. Bilbao, Kinetic modelling of dimethyl ether synthesis from (H2+CO2) by considering catalyst deactivation, Chem. Eng. J. 174 (2–3) (2011) 660–667, https://doi.org/10.1016/j.cej.2011.09.067.
[35] R. Peláez, P. Marín, S. Ordóñez, Direct synthesis of dimethyl ether from syngas over mechanical mixtures of CuO/ZnO/Al2O3 and γ-Al2O3: process optimization and

kinetic modelling, Fuel Process. Technol. 168 (2017) 40–49, https://doi.org/10.1016/j.fuproc.2017.09.004.
[36] N. Delgado Otalvaro, M. Kaiser, K. Herrera Delgado, S. Wild, J. Sauer, H. Freund, Optimization of the direct synthesis of dimethyl ether from CO2 rich synthesis gas: closing the loop between experimental investigations and model-based reactor design, Reaction Chemistry & Engineering 5(5) (2020) 949-960. https://doi.org/10.1039/d0re00041h.
[37] Y.T. Kim, K.-D. Jung, E.D. Park, A comparative study for gas-phase dehydration of glycerol over H-zeolites, Appl. Catal. A 393 (1–2) (2011) 275–287, https://doi.org/10.1016/j.apcata.2010.12.007.
[38] B. Lacerda de Oliveira Campos, K. Herrera Delgado, S. Wild, F. Studt, S. Pitter, J. Sauer, Surface reaction kinetics of the methanol synthesis and the water gas shift reaction on Cu/ZnO/Al2O3, Reaction Chemistry & Engineering 6(5) (2021) 868-887. https://doi.org/10.1039/d1re00040c.
[39] T. Fujitani, I. Nakamura, T. Uchijima, J. Nakamura, The kinetics and mechanism of methanol synthesis by hydrogenation of CO2 over a Zn-deposited Cu(111) surface, Surf. Sci. 383 (2–3) (1997) 285–298, https://doi.org/10.1016/s0039-6028(97)00192-1.
[40] J.D. Grunwaldt, A.M. Molenbroek, N.Y. Topsøe, H. Topsøe, B.S. Clausen, In situ investigations of structural changes in Cu/ZnO Catalysts, J. Catal. 194 (2) (2000) 452–460, https://doi.org/10.1006/jcat.2000.2930.
[41] S. Kuld, M. Thorhauge, H. Falsig, C.F. Elkjaer, S. Helveg, I. Chorkendorff, J. Sehested, Quantifying the promotion of Cu catalysts by ZnO for methanol synthesis, Science 352 (6288) (2016) 969–974, https://doi.org/10.1126/science.aaf0718.
[42] C.V. Ovesen, B.S. Clausen, J. Schiøtz, P. Stoltze, H. Topsøe, J.K. Nørskov, Kinetic implications of dynamical changes in catalyst morphology during methanol synthesis over Cu/ZnO catalysts, J. Catal. 168 (2) (1997) 133–142, https://doi.org/10.1006/jcat.1997.1629.
[43] H.S. Fogler, Elements of Chemical Reaction Engineering, Prentice Hall PTR2006.
[44] T. Lunkenbein, F. Girgsdies, T. Kandemir, N. Thomas, M. Behrens, R. Schlogl, E. Frei, Bridging the time gap: a copper/zinc oxide/aluminum oxide catalyst for methanol synthesis studied under industrially relevant conditions and time scales, Angew Chem Int Ed Engl 55 (41) (2016) 12708–12712, https://doi.org/10.1002/anie.201603368.
[45] G. James, D. Witten, T. Hastie, R. Tibshirani, An Introduction to Statistical Learning, 2 ed., Springer New York2021. https://doi.org/10.1007/978-1-0716-1418-1.
[46] A. Karelovic, G. Galdames, J.C. Medina, C. Yévenes, Y. Barra, R. Jiménez, Mechanism and structure sensitivity of methanol synthesis from CO2 over SiO2-supported Cu nanoparticles, J. Catal. 369 (2019) 415–426, https://doi.org/10.1016/j.jcat.2018.11.012.
[47] B. Lacerda de Oliveira Campos, K. John, P. Beeskow, K. Herrera Delgado, S. Pitter, N. Dahmen, J. Sauer, A detailed process and techno-economic analysis of methanol synthesis from h2 and co2 with intermediate condensation steps, Processes 10 (8) (2022), https://doi.org/10.3390/pr10081535.
[48] M. Semmel, M. Kerschbaum, B. Steinbach, J. Sauer, O. Salem, Optimized design and techno-economic analysis of novel DME production processes, React. Chem. Eng. 8 (11) (2023) 2826–2840, https://doi.org/10.1039/d3re00333g.
[49] A. Praśnikar, A. Pavlišič, F. Ruiz-Zepeda, J. Kovač, B. Likozar, Mechanisms of copper-based catalyst deactivation during co2 reduction to methanol, Ind. Eng. Chem. Res. 58 (29) (2019) 13021–13029, https://doi.org/10.1021/acs.iecr.9b01898.
[50] J. Wu, M. Saito, M. Takeuchi, T. Watanabe, The stability of Cu/ZnO-based catalysts in methanol synthesis from a CO2-rich feed and from a CO-rich feed, Appl. Catal. A 218 (1–2) (2001) 235–240, https://doi.org/10.1016/s0926-860x(01)00650-0.